Predictions of Separated and Transitional Boundary Layers Under Low-Pressure Turbine Airfoil Conditions Using an Intermittency Transport Equation

Y. B. Suzen
Senior Engineer Associate

P. G. Huang
Professor

Department of Mechanical Engineering,
University of Kentucky,
Lexington, KY 40506-0503

Lennart S. Hultgren
Aerospace Engineer
Mem. ASME

David E. Ashpis
Aerospace Engineer

National Aeronautics and Space Administration,
Glenn Research Center at Lewis Field,
Cleveland, OH 44135

A new transport equation for the intermittency factor was proposed to predict separated and transitional boundary layers under low-pressure turbine airfoil conditions. The intermittent behavior of the transitional flows is taken into account and incorporated into computations by modifying the eddy viscosity, μ_t, with the intermittency factor, γ. Turbulent quantities are predicted by using Menter's two-equation turbulence model (SST). The intermittency factor is obtained from a transport equation model, which not only can reproduce the experimentally observed streamwise variation of the intermittency in the transition zone, but also can provide a realistic cross-stream variation of the intermittency profile. In this paper, the intermittency model is used to predict a recent separated and transitional boundary layer experiment under low pressure turbine airfoil conditions. The experiment provides detailed measurements of velocity, turbulent kinetic energy and intermittency profiles for a number of Reynolds numbers and freestream turbulent intensity conditions and is suitable for validation purposes. Detailed comparisons of computational results with experimental data are presented and good agreements between the experiments and predictions are obtained. [DOI: 10.1115/1.1580159]

1 Introduction

Flow transition plays an important role in turbomachinery applications. Majority of boundary layer flows in turbomachines involve flow transition under the effects of freestream turbulence, diverse pressure gradients, wide range of Reynolds numbers, flow separation, and unsteady wake-boundary layer interactions.

Prediction of this type of complex flows is an important element in analysis and performance evaluation of gas turbine engine components and ultimately in the design of more efficient jet engines. Especially, in low-pressure turbine applications prediction of transition behavior is even more important for reasons of design efficiency. For low-pressure turbines the flow is mostly turbulent at the high Reynolds number conditions encountered at take-off and the efficiency is at its design maximum. However, due to decrease of Reynolds number caused by high altitude conditions at cruise speeds, design based on the sea level conditions tends to underpredict losses and thus leads to substantial drops in efficiency [1–3]. These losses are attributed to flow separation on the suction surface of the turbine blades. At low Reynolds numbers with low freestream turbulence, the boundary layers on the airfoil surface have a tendency to remain laminar and hence the flow may separate before it becomes turbulent. This may cause a drop in efficiency and result in increase of fuel consumption. The impact of such losses is directly felt on the operation costs. It has been estimated that a 1% improvement in the efficiency of a low pressure turbine would result in a saving of $52,000 per year on a typical airliner [4].

In order to calculate the losses and heat transfer on various components of gas turbine engines, and to be able to improve component efficiencies and reduce losses through better designs, accurate prediction of development of transitional boundary layers is essential [1]. For an accurate prediction of transitional flows under the diverse conditions encountered in turbomachinery applications, the aim is to find a model providing the following properties:

- Physically accurate and versatile: The model should be capable of accurately predicting transitional flows under the diverse conditions encountered in turbomachinery applications, such as pressure gradients, freestream turbulence, wide range of Reynolds numbers, unsteady wake-boundary layer interactions and flow separation.
- Computationally efficient and inexpensive: The model should not involve extensive computational effort and should be relatively cheap to compute.
- Compatible with current CFD methods: The model should be easy to implement into existing CFD codes without requiring extensive changes in computational strategy.

One of the current methods for predicting flow transition is to use the stability theory. In this method, stability equations are solved at streamwise stations in order to predict the onset of transition. This method requires prior solution of the mean flow field and returns only the onset point of transition without any information on the turbulent part of the flow. Another method is using empirical correlations in the form of e^n. This type of methods also require prior solution of the mean flow field. These two methods are not compatible with current CFD methods.

One method compatible with current CFD methods is the use of low-Reynolds number turbulence models. Savill [5,6], has organized a number of workshops to assess the capability of current turbulence models in predicting flow transition. The comparisons showed that none of the existing models was adequate to predict flow transition for a range of flow conditions. Westin and Henkes [7] have also tested a large variety of turbulence models and compared models' performances in predicting a few of the T3-series transition flow experiments [5]. They indicated that none of the models could predict both onset location and length of transition

Contributed by the International Gas Turbine Institute for publication in the JOURNAL OF TURBOMACHINERY. Manuscript received by the IGTI July 9, 2001; revised manuscript received March 10, 2003. Associate Editor: S. Sjolander.

for a range of flow conditions. This outcome is not at all surprising since most of the current turbulence models are not designed to predict flow transition.

An alternative method to this approach is to use the concept of intermittency to blend the flow from the laminar to the turbulent regions. This approach, although highly empirical, has shown some successes in predicting transition behavior. Dhawan and Narasimha [8] correlated the experimental data and proposed a generalized intermittency distribution function across flow transition. The correlation was later improved by Gostelow et al. [9] for flows with pressure gradients subject to a range of freestream turbulence intensities.

Solomon et al. [10], following the work of Chen and Thyson [11], developed an improved method to predict transitional flows involving changes in pressure gradients. In this model, the effects of changing streamwise pressure gradient on the breakdown physics and spot spreading rates are taken into account. This is accomplished by varying the spot spreading angle and propagation parameter through the transition zone according to the local pressure gradient parameter.

Steelant and Dick [12] proposed a transport equation for intermittency, in which the source term of the equation is developed such that the γ distribution of Dhawan and Narasimha [8] across the transition region can be reproduced. Steelant and Dick used their model, coupled with two sets of conditioned Navier-Stokes equations, to predict transitional flows with zero, favorable, and adverse pressure gradients. However, since their technique involved the solution of two sets of strongly coupled equations, the method is not compatible with existing CFD codes, in which only one set of Navier-Stokes equations is involved. Moreover, the model was designed to provide a realistic streamwise γ behavior but with no consideration of the variation of γ in the cross-stream direction.

Cho and Chung [13] developed a $k-\epsilon-\gamma$ turbulence model for free shear flows. Their turbulence model explicitly incorporates the intermittency effect into the conventional $k-\epsilon$ model equations by introducing an additional transport equation for γ. They applied this model to compute a plane jet, a round jet, a plane far wake, and a plane mixing layer with good agreements. Although this method was not designed to reproduce flow transition, it provided a realistic profile of γ in the cross-stream direction.

Suzen and Huang [14] improved the intermittency transport equation by combining the best properties of Steelant and Dick's model and Cho and Chung's model. Their model reproduces the streamwise intermittency distribution of Dhawan and Narasimha [8] and also produces a realistic variation of intermittency in the cross-stream direction. The model is capable of predicting flow transition under diverse conditions. The predicting capabilities of this model have been validated against T3-series experiments of Savill [5,6] and low-pressure turbine experiments of Simon et al. [15] with good success [14,16,17].

In the current research we focus on further validation of the intermittency transport model of Suzen and Huang [14] against the experiments of Hultgren and Volino [18]. Hultgren and Volino's experiments investigated the effects of freestream turbulence and Reynolds number on separated and transitional boundary layers under low-pressure turbine airfoil conditions. In their experiments, a flat plate boundary layer subject to a streamwise pressure gradient was studied. The superimposed pressure gradients were produced by attaching a two-dimensional contoured shape to the wall opposite to the test surface and by applying suction on the contoured wall. The resultant pressure profile represents that on the suction side of the Pak-B airfoil. The experiments covered a range of flow conditions including Reynolds numbers between 50,000 and 300,000 and freestream turbulence intensities between 0.2 and 7%. These cases cover a realistic range of operating conditions from take-off to cruise. On the test wall, velocity, turbulent kinetic energy and intermittency profiles were measured at 14 streamwise stations. In the measurements, quantities such as skin friction coefficients, transition start and end locations, and the locations of separation and reattachment were also determined. Further details of the measurements and experimental data were given by Volino and Hultgren [19].

The experiments of Hultgren and Volino [18] provide a good set of data for the development and validation of the models for flow transition. In the next section, the intermittency transport model is presented and implementation of the model is described along with the empirical correlations employed for the onset of transition. In Section 3, the numerical details of the prediction process are given. In Section 4, the predictions of the new intermittency model are compared against the experimental data. Finally, conclusions are provided in Section 5.

2 Transport Model for the Intermittency

In this section, the transport model for intermittency is presented. The model combines the transport equation models of Steelant and Dick [12] and Cho and Chung [13]. Details of the development and implementation of the transport model are given in Suzen and Huang [14,16], Suzen et al. [17].

The model equation is given by

$$\frac{\partial \rho\gamma}{\partial t}+\frac{\partial \rho u_j\gamma}{\partial x_j}=(1-\gamma)\Bigg[(1-F)2C_0\rho\sqrt{u_k u_k}f(s)f'(s)+F\Bigg(\frac{C_1\gamma}{k}\tau_{ij}\frac{\partial u_i}{\partial x_j}-C_2\gamma\rho\frac{k^{3/2}}{\epsilon}\times\frac{u_i}{(u_k u_k)^{1/2}}\frac{\partial u_i}{\partial x_j}\frac{\partial\gamma}{\partial x_j}\Bigg)\Bigg]+C_3\rho\frac{k^2}{\epsilon}\frac{\partial\gamma}{\partial x_j}\frac{\partial\gamma}{\partial x_j}+\frac{\partial}{\partial x_j}\times\Bigg(((1-\gamma)\gamma\sigma_{\gamma l}\mu+(1-\gamma)\sigma_{\gamma t}\mu_t)\frac{\partial\gamma}{\partial x_j}\Bigg) \quad (1)$$

The distributed breakdown function, $f(s)$ has the form

$$f(s)=\frac{as'^4+bs'^3+cs'^2+ds'+e}{gs'^3+h} \quad (2)$$

where $s'=s-s_t$, s is the distance along the streamline coordinate, and s_t is the transition location. The coefficients are

$$a=50\sqrt{\frac{n\sigma}{U}}\quad b=-0.4906\quad c=0.204\left(\frac{n\sigma}{U}\right)^{-0.5}$$
$$d=0.0\quad e=0.04444\left(\frac{n\sigma}{U}\right)^{-1.5} \quad (3)$$
$$h=10e\quad\text{and}\quad g=50$$

The shear stresses are defined as

$$\tau_{ij}=\mu_t\left[\frac{\partial u_i}{\partial x_j}+\frac{\partial u_j}{\partial x_i}-\frac{2}{3}\frac{\partial u_k}{\partial x_k}\delta_{ij}\right]-\frac{2}{3}\rho k\delta_{ij} \quad (4)$$

The blending function F is constructed using a nondimensional parameter, k/Wv, where k is the turbulent kinetic energy and W is the magnitude of the vorticity. The blending function has the form

$$F=\tanh^4\left[\frac{k/Wv}{200(1-\gamma^{0.1})^{0.3}}\right] \quad (5)$$

The model constants used in Eq. (1) are

$$\sigma_{\gamma l}=\sigma_{\gamma t}=1.0\quad C_0=1.0\quad C_1=1.6$$
$$C_2=0.16\quad\text{and}\quad C_3=0.15$$

The intermittency is incorporated into the computations simply by multiplying the eddy viscosity obtained from a turbulence model, μ_t, by the intermittency factor, γ. Simon and Stephens [20] showed that by combining the two sets of conditioned

Navier-Stokes equations and making the assumption that the Reynolds stresses in the nonturbulent part are negligible, the intermittency can be incorporated into the computations by using the eddy viscosity, μ_t^*, which is obtained by multiplying the eddy viscosity from a turbulence model, μ_t, with the intermittency factor, γ; that is,

$$\mu_t^* = \gamma \mu_t \tag{6}$$

is used in the mean flow equations. It must be noted that γ does not appear in the generation term of the turbulent kinetic energy equations.

The intermittency model had been implemented into TURCOM code developed by Huang and Coakley [21] and validated against low-pressure turbine experiments of Simon et al. [15] in Suzen et al. [17].

It is essential that the turbulence model selected to obtain μ_t must produce fully turbulent features before transition location in order to allow the intermittency to have full control of the transitional behavior. Menter's [22] SST model satisfies this requirement. It produces almost fully turbulent flow in the leading edge of the boundary layer and therefore it is used as a baseline model to compute μ_t and other turbulent quantities in the computations [17].

The value of $n\sigma$ used in evaluating the constants given by Eq. (3) is provided by the following correlation for zero pressure gradient flows [17]:

$$\hat{n}\sigma = (n\nu^2/U^3)\sigma = 1.8\times 10^{-11}\mathrm{Tu}^{7/4} \tag{7}$$

When flows are subject to pressure gradients, the following correlation is used:

$$\frac{\hat{n}\sigma}{(\hat{n}\sigma)_{ZPG}} = \begin{cases} M^{(1-\exp(0.75\times 10^6 K_t \mathrm{Tu}^{-0.7}))}, & K_t<0 \\ 10^{-3227K_t^{0.5985}}, & K_t>0 \end{cases} \tag{8}$$

with M defined as:

$$M = (850\mathrm{Tu}^{-3} - 100\mathrm{Tu}^{-0.5} + 120)$$

where $(\hat{n}\sigma)_{ZPG}$ is the value for flow at zero pressure gradient and can be obtained from Eq. (7) and $K_t = (\nu/U_t^2)(dU/dx)_t$ is the flow acceleration parameter. The favorable pressure gradient part of the foregoing correlation (for $K_t>0$) is from Steelant and Dick [12]. The portion of the correlation for adverse pressure gradient flows, $K_t<0$, is formulated using the transition data of Gostelow et al. [9] and Simon et al. [15] in Suzen et al. [17].

The current approach uses the intermittency transport model to obtain the intermittency distribution for the transitional flows, while the onset of transition is defined by the correlations discussed in the next section.

Attached-Flow Transition. Abu-Ghannam and Shaw [23] suggested that the onset of transition for attached flows can be obtained by correlating the boundary layer momentum thickness Reynolds number to the freestream turbulence intensity according to

$$\mathrm{Re}_{\theta t} = 163 + \exp\left[F(\lambda_\theta) - \frac{F(\lambda_\theta)}{6.91}\mathrm{Tu}\right] \tag{9}$$

where

$$F(\lambda_\theta) = 6.91 + 12.75\lambda_\theta + 63.64\lambda_\theta^2 \quad \text{for } \lambda_\theta<0, \text{ or}$$

$$F(\lambda_\theta) = 6.91 + 2.48\lambda_\theta - 12.27\lambda_\theta^2 \quad \text{for } \lambda_\theta>0$$

Although Abu-Ghannam and Shaw correlation shows good agreement with experimental data for flows with zero and adverse pressure gradients, the model is not very sensitive to flows subject to strong favorable pressure gradients, in which one would expect the transition to be delayed as a result of flow acceleration [17].

To allow for a more sensitive response to strong favorable pressure gradients while maintaining the good features of Abu-Ghannam and Shaw in adverse pressure gradient region, the transition criterion was re-correlated to the freestream turbulence intensity, Tu, and the acceleration parameter, K_t,

$$\mathrm{Re}_{\theta t} = (120 + 150\mathrm{Tu}^{-2/3})\coth[4(0.3 - K_t\times 10^5)] \tag{10}$$

where K_t was chosen as the maximum absolute value of that parameter in the downstream deceleration region [17]. Equation (10) was designed to have a better fit of the available experimental data: while the correlation fits the transition data well for flows under adverse pressure gradients, it was purposely designed to rise rapidly as K_t becomes positive. This measure is to reflect the fact that the flow becomes less likely to have transition when subject to favorable pressure gradients.

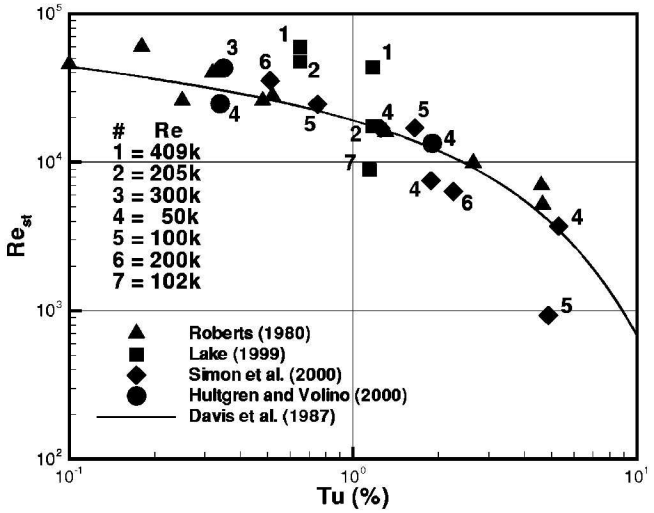

Fig. 1 Onset of separated flow transition

Separated-Flow Transition. Roberts [24] proposed a semi-empirical theory to predict onset of transition within a laminar separation bubble over the airfoil suction surface. The transition Reynolds number, Re_{st}, which is based on the length defined between the onset location of separation and that of transition, is correlated as a function of a turbulent factor representing effects of the external turbulence level and its disturbance spectrum. The model was simplified by Davis et al. [25] to only a function of turbulence intensity,

$$\mathrm{Re}_{st} = 2.5\times 10^4 \log_{10}\coth(0.1732\mathrm{Tu}) \tag{11}$$

where Tu is the freestream turbulence intensity value at the onset of separation. Although this model was originally proposed for swept wing flows, it had been used widely for predicting onset of transition in a variety of separated flows. However, comparisons of recently available data for onset of transition in separated flows suggest that the correlation for the onset of transition is better represented by a function of more than one parameter.

In Fig. 1, Davis et al. [25] correlation is given along with the data of Roberts [24] (the original data used to develop Davis' correlation), Simon et al. [15], Hultgren and Volino [18] and Lake [26]. Each point (except for the data of Roberts [24]) is numbered to indicate the Reynolds numbers of the cases based on exit velocity and suction surface length. There is some scatter in the data especially for high Reynolds number cases of Lake [26]. In order to capture the scatter of the data, we incorporated the effect of Reynolds number into the correlation for Re_{st}. The new correlation expresses Re_{st} in terms of the turbulence intensity (Tu) and the momentum thickness Reynolds number at the point of separation ($\mathrm{Re}_{\theta s}$) and is given as;

$$\mathrm{Re}_{st} = 874\,\mathrm{Re}_{\theta s}^{0.71}\exp[-0.4\mathrm{Tu}] \tag{12}$$

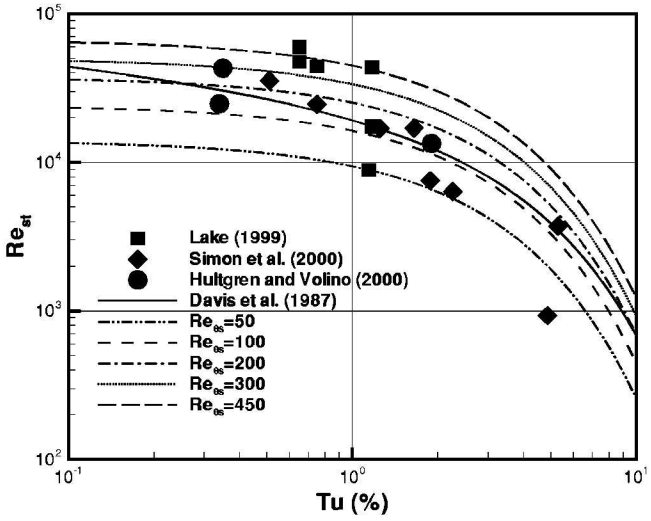

Fig. 2 Onset of separated flow transition with new correlation (Eq. 12)

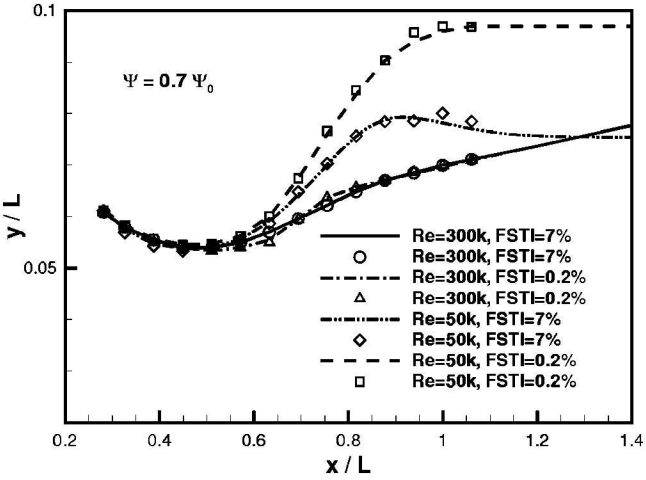

Fig. 4 Outer boundary shapes for all cases

In Fig. 2, the new correlation is compared with the experimental data for different values of $Re_{\theta s}$. In contrast to Davis et al. [25] correlation, the current formula seems to provide a better representation of the data scattering. In the present paper Eq. (12) is used as a replacement of Davis et al. correlation to predict the onset of separated-flow transition.

3 Numerical Details

As mentioned earlier, the experiments made use of a flow suction on the upper (contoured) surface to arrive at the desired pressure distribution. Although the shape of the upper contoured surface is known, no information is available for the conditions of the suction on this surface. This somewhat makes the computation of the problem ill-posed. In order to provide the upper boundary of the computational domain, we defined a prescribed streamline, obtainable by integrating the experimental measured velocity profiles, as the upper boundary. Once the streamline is defined as the upper computational boundary, a slip boundary condition can be applied at the upper surface.

For example, in Fig. 3 the streamlines obtained by using different values of

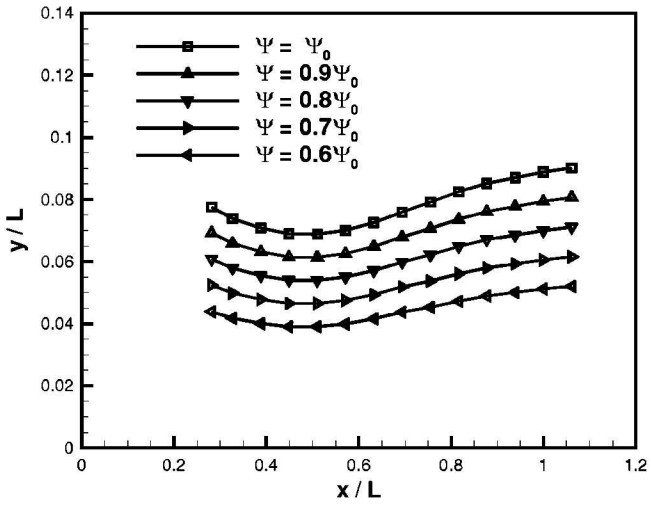

Fig. 3 Streamlines from experimental data, Re=300,000, FSTI=7%

$$\Psi = \int_0^h u\,dy, \tag{13}$$

are presented for the case with Re=300,000 and FSTI=7%. In this figure Ψ_0 is the Ψ obtained from Eq. (13) at the first station taking h as the maximum height of the measured y position. To define the streamlines, we performed the integration of measured velocity profiles based on Eq. (13) in all x stations such that Ψ is a constant. Any one of the streamlines shown in Fig. 3 can be used as the outer boundary of the computational domain, as long as they are well outside the boundary layer. Similar streamline curves can be generated for other cases.

In the computations, we selected a streamline corresponding to $\Psi = 0.7\Psi_0$ as the upper boundary of the computational domain. The shapes of the upper streamlines are presented in Fig. 4 for all of the cases considered. In this figure the symbols show the points obtained from integration of the experimental velocity profiles and the lines indicate the boundary shapes used in the computations. By varying different streamline positions, we have found the streamline corresponding to $\Psi = 0.7\Psi_0$ is sufficiently remote from the boundary layer to be considered as freestream. The boundary layer edge at each axial station is taken to be the location where the velocity is 99% of the maximum streamwise velocity at that station. Nonuniform meshes consisting of 140×60 grid points are used for all calculations. All grids have first y^+ values less than 0.5. A grid refinement study for the case with Re=50,000 and FSTI=7% (using a 250×100 mesh) has revealed that the solution obtained by the current mesh can be accepted as a grid independent solution.

Although the last experimental station is located at $x/L = 1.06$, the computational domain is extended to $x/L = 1.4$ in the streamwise direction to allow the outflow boundary condition to be applied in the computations. We have extended the upper streamline boundary up to $x/L = 1.25$ and a constant pressure outflow boundary conditions is applied downstream of that station. Although this extension of the domain may appear to be arbitrary, it is necessary to avoid having reversed flow close to the exit boundary. Since no reverse flow was encountered for all cases after $x/L \approx 1.25$, the extension of the domain up to $x/L = 1.4$ seems reasonable. The plate surface is assumed to be an adiabatic wall and a constant-pressure outflow boundary condition is applied on the exit plane for all cases.

In order to obtain accurate inlet profiles for the computations, a laminar computation over a flat plate is performed. From this computation, the profile matching the momentum thickness the first experimental station is extracted as the inlet condition for the computations.

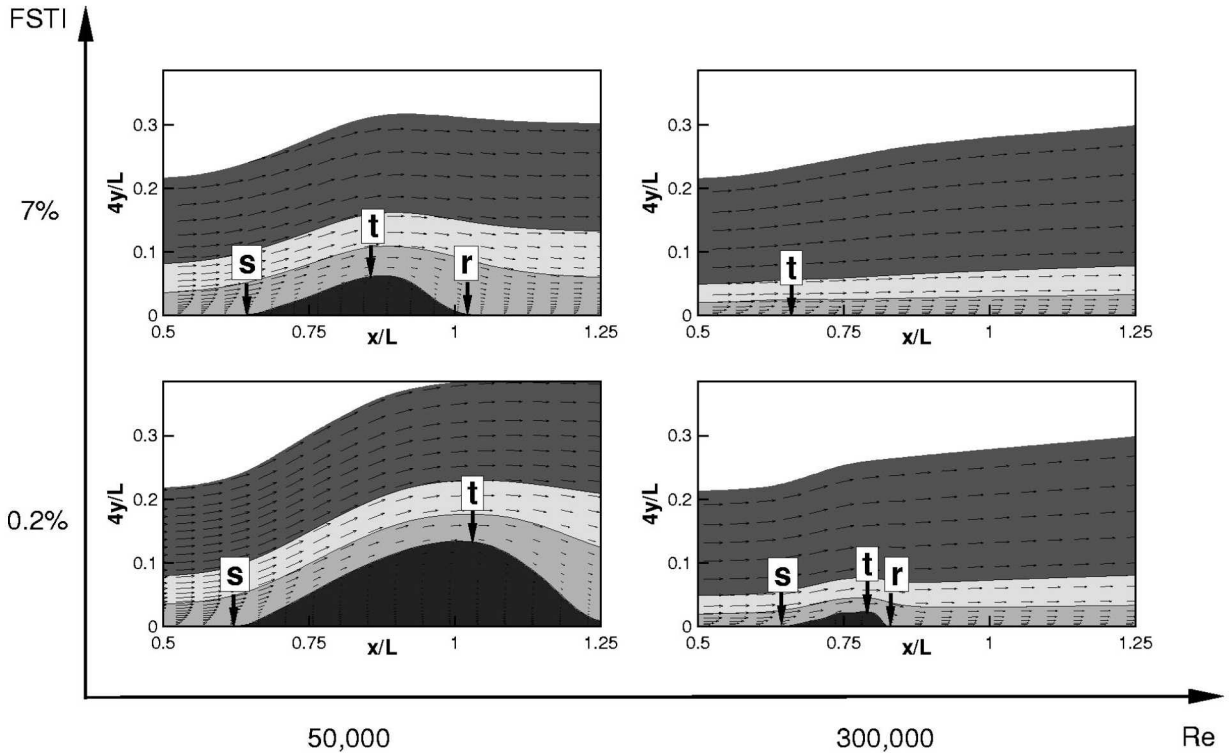

Fig. 5 Overall view of effects of Reynolds number and freestream turbulence intensity

4 Results and Discussion

In this section the comparison of the predictions with experimental data of Hultgren and Volino [18] are presented.

The experiment considered in this study involves two different Reynolds numbers, Re=300,000 and Re=50,000 (based on nominal exit velocity, U_{ref}, and wetted plate length, $L=0.208$ m) and two freestream turbulence intensities, FSTI=7% and FSTI=0.2%. Figure 5 depicts the dynamic interplay between transition and separation when subject to variations in Reynolds number and freestream turbulence effects. In this figure the insets **s** and **t** denote the onset of separation and transition, respectively, and the inset **r** denotes the reattachment point. The first case considered is with Re=300,000 and FSTI=7%. For this case, the transition position is at $x/L=0.66$ and only a tiny flow separation is observed near $x/L\approx0.7$. As the Reynolds number is decreased from 300,000 to 50,000 while keeping the freestream turbulence intensity the same, the onset of transition is delayed until $x/L=0.85$. As a result of the delay of the transition, a sizable flow separation is encountered between $x/L\approx0.65$ and ≈1.0. On the other hand, when the turbulence intensity is decreased from 7 to 0.2% while the Reynolds number is maintained at 300,000, the transition onset is delayed until $x/L\approx0.79$. As a result, a small but visible separation bubble is observed in the vicinity of $x/L\approx0.75$. The last case involved a simultaneous decrease of Reynolds number and freestream turbulence intensity, from 300,000 to 50,000 and from 7 to 0.2%, respectively. In this case the onset of transition is delayed to $x/L\approx1.03$ and a massive separation extending from $x/L\approx0.65$ to ≈1.25 is observed. The current prediction is an attempt to mimic the aforementioned dynamic behavior of the interaction between transition and separation when subject to changes in Reynolds number and freestream turbulence intensity conditions.

For the case involving Re=300,000 and FSTI=7%, experimental onset point of transition is at $Re_\theta=336$ which corresponds to a location $x/L=0.66$. However, the onset point of transition for this case seems to be higher than other experimental data trend compiled by Mayle [1] and Savill [5] and also higher than the value given by the correlation of Abu-Ghannam and Shaw [23]. For example, the freestream turbulence intensity at the point of transition is Tu=1.7% and the acceleration parameter is, $K_t=-2.5\times10^{-6}$, by applying Eq. (10), the predicted onset location is much earlier (at $Re_\theta=230$, corresponding to $x/L=0.55$). To show the effect of the transition positions, we have performed two different computations for this case: one using the experimental onset point of transition and the other using the onset point obtained from the correlation, Eq. (10).

The predicted pressure coefficient distribution along the surface is compared with experimental data, as shown in Fig. 6(*a*). In this figure, the results of the computation using the experimental onset of transition point is titled as "Computation 1" and the one obtained by utilizing Eq. (10) is denoted as "Computation 2." Both results show very good agreements with experimental data and only slight differences in the distributions near $x/L\approx0.65$ are observed between the two computations.

The velocity profiles for the two computations are compared with experimental data in Figs. 6(*b*) and (*c*). In the experiment, the flow remains laminar before station $x/L=0.69$. At station $x/L=0.69$ the velocity profile indicates that the flow is on the verge of separation. At the next station ($x/L=0.75$), the boundary layer is attached and the flow continues to develop as an attached turbulent boundary layer. Although it is not seen from the measured velocity profiles, it was reported experimentally that a very small separation region exists between the two measured stations, $x/L=0.69$ and 0.75. In contrast, no separation was observed in both computations although the comparison of the velocity profiles shows the predictions agree very well with experimental data. Both computations produce similar results except in the region $x/L\approx0.7$. Due to the fact that the onset point of transition of computation 2 is slightly upstream, the result of computation 2 is fuller and is less likely to separate than that of computation 1; otherwise, the differences between the two profiles are small.

The intermittency profiles of the two computations are compared with experimental data in Figs. 7(*a*) and (*b*). As can be seen from Fig. 7*a*, the flow is laminar at the first seven stations. In both

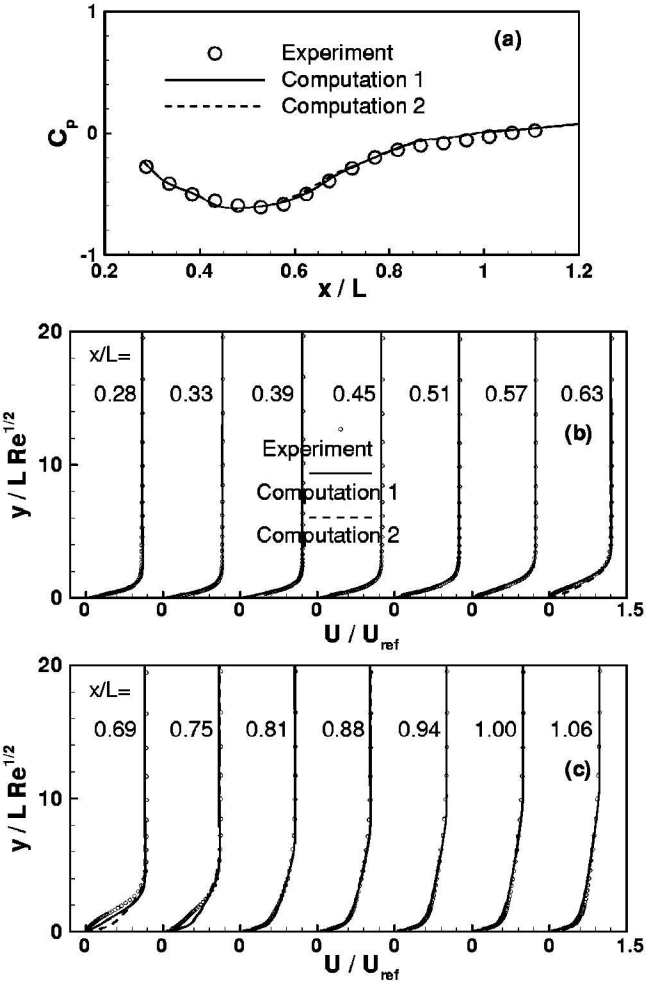

Fig. 6 Prediction of experiment of Hultgren and Volino [18]—Re=300,000, FSTI=7%

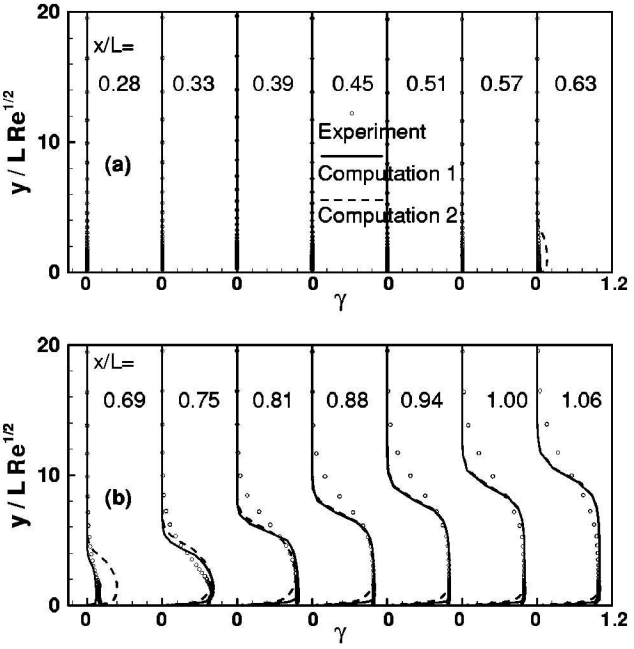

Fig. 7 Comparison of intermittency profiles along the surface—Re=300,000, FSTI=7%

the experiment and the computation 1, transition begins at station $x/L=0.66$ and in computation 2 the transition starts at $x/L=0.55$. While the transition of the computation 2 is ahead of the computation 1, the length of transition is somewhat longer due to the fact that a small value of spot generation rate, $n\sigma$, is calculated. The maximum value of the intermittency in the profiles of computation 1 reaches unity near station $x/L=0.81$ whereas in computation 2, the intermittency reaches unity only after $x/L=0.88$. Overall, computation 1 shows slightly better agreement with experiments than computation 2 even though the differences of the two results are mainly limited to the near wall region.

In Figs. 8(*a*) and (*b*), comparisons of the turbulent kinetic energy profiles are made. As can be seen from these figures, the freestream decay of turbulent kinetic energy throughout the plate is made to match the decay of freestream turbulence. This match provides the initial conditions for dissipation of the turbulent kinetic energy (see Suzen and Huang [14], for details). The predicted profiles of the turbulent kinetic energy seem to follow the experimental trend well even though the values are slightly larger before $x/L=0.7$ and smaller after that. Again, the differences of the two computations were only limited to region near $x/L=0.7$.

The next case considered involves the same freestream turbulence intensity (FSTI=7%) while Reynolds number is reduced from 300,000 to 50,000. In the experiment, the flow separated at $x/L=0.63$ and the onset of transition was observed at $x/L=0.85$. In the computations, separation took place at $x/L=0.66$ and the onset point of transition calculated from Eq. (12) was at $x/L=0.88$. The pressure coefficient distribution is compared with experimental data, as shown in Fig. 9(*a*). The agreement with the experimental data is good except in the region after $x/L=0.95$, where it can be seen that the pressure coefficient is slightly underpredicted indicating that the streamwise velocity distribution is slightly overpredicted.

The comparisons of the velocity profiles are given in Figs. 9(*b*) and (*c*). The profiles are in good agreement with the experiment up to $x/L=0.88$. The experimental data shows that the flow attaches after $x/L=0.94$ whereas the predictions indicate that the separation is extended up to $x/L=1.0$.

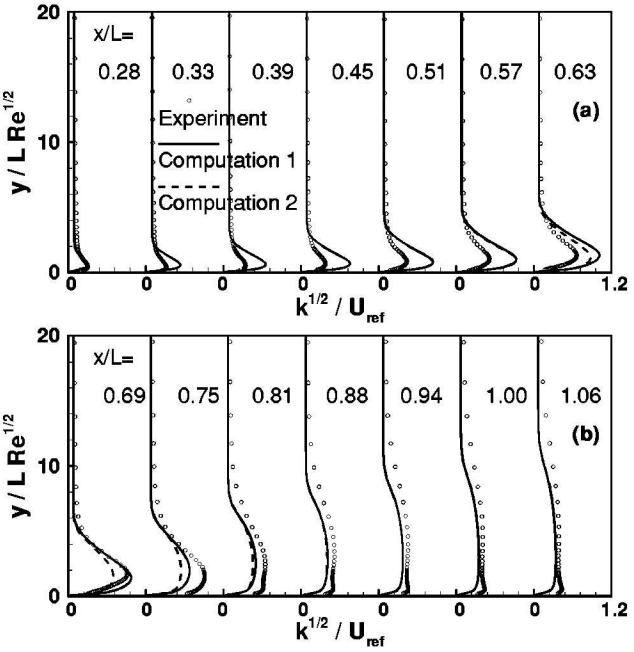

Fig. 8 Comparison of turbulence intensity profiles along the surface—Re=300,000, FSTI=7%

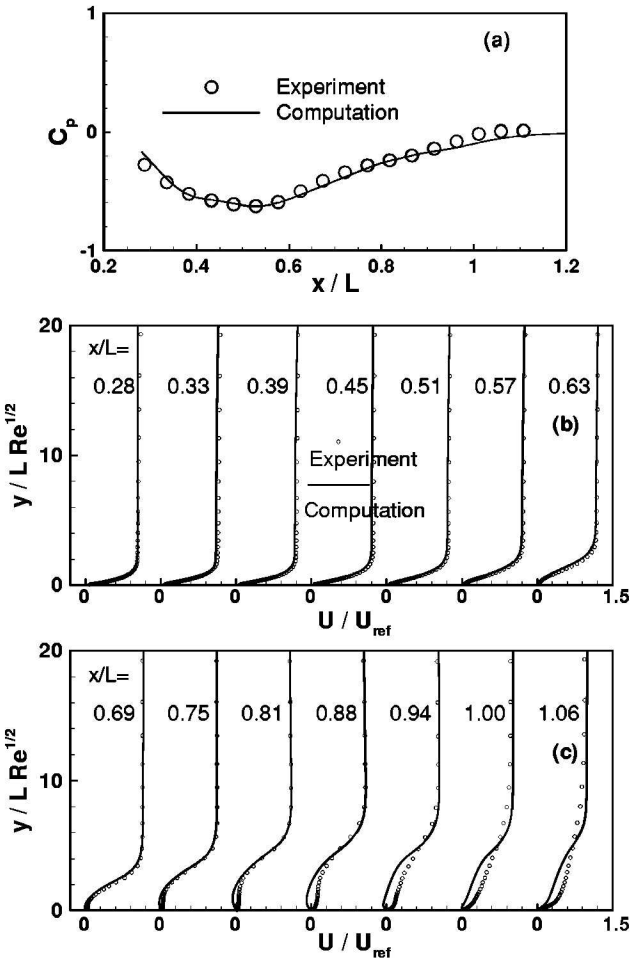

Fig. 9 Prediction of experiment of Hultgren and Volino [18]—Re=50,000, FSTI=7%

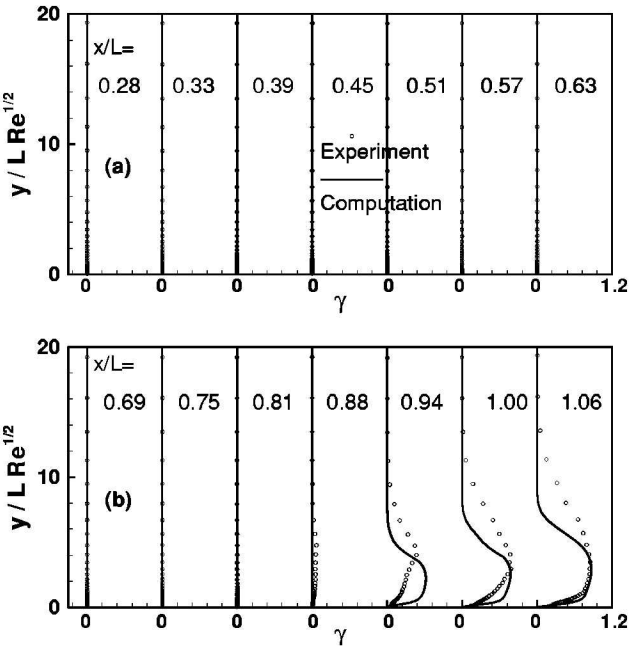

Fig. 10 Comparison of intermittency profiles along the surface—Re=50,000, FSTI=7%

The intermittency profiles are compared to experimental data in Figs. 10(*a*) and (*b*). The general profile trend is well predicted even though the exact profile shapes are not well captured. In Figs. 11(*a*) and (*b*), comparisons of turbulence intensity profiles are shown. It can be seen that the comparisons between the predictions and experimental data are favorable.

The next case involves FSTI=0.2% and Re=300,000. In the experiment, the flow separated at $x/L=0.67$, and the transition onset was observed between stations $x/L=0.75$ and $x/L=0.81$. The prediction shows that separation was at $x/L=0.66$ and the onset of transition (obtained from Eq. (12)) was at $x/L=0.79$. The comparison of the pressure coefficient distribution is presented in Fig. 12(*a*). The computed profile shows very good agreement with the experimental data.

The comparison of the velocity profiles are given in Figs. 12(*b*) and (*c*). The agreement between the predictions and experimental data is very good. It should be noted that there seems to be some discrepancies between the prediction and the measurement in the near-wall region near the flow separation region ($x/L\approx0.8$), this difference is caused by the failure of the hot wire measurement for the flow reversal.

The intermittency profiles are compared to experimental data in Figs. 13(*a*) and (*b*). The trend for the streamwise development of the intermittency factors seems to be well predicted, even though the model predicts a less diffusive behavior of the intermittency profiles near the freestream region.

The turbulence intensity profiles along the surface are compared to experimental data in Figs. 14(*a*) and (*b*). Although the general trend of the turbulent kinetic energy profiles is captured, it can be seen that the prediction gives rise to larger values of the turbulence kinetic energy for flow up to $x/L\approx0.85$.

Finally, both Reynolds number and the freestream turbulence intensity are decreased to 50,000 and to 0.2%, respectively. For this case, flow separation was observed at $x/L=0.63$ and the onset of transition was observed between stations $x/L=1.0$ and 1.06 in the experiment. The flow did not reattach at the last measured station ($x/L=1.06$). The predictions indicate that the flow separation is at $x/L=0.64$ and the onset of transition calculated from Eq. (12) is at $x/L=1.03$. The predicted pressure coefficient distri-

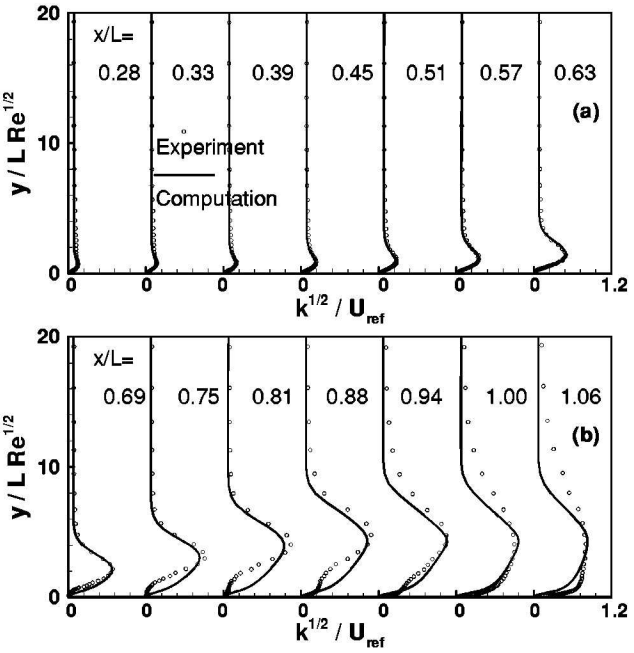

Fig. 11 Comparison of turbulence intensity profiles along the surface—Re=50,000, FSTI=7%

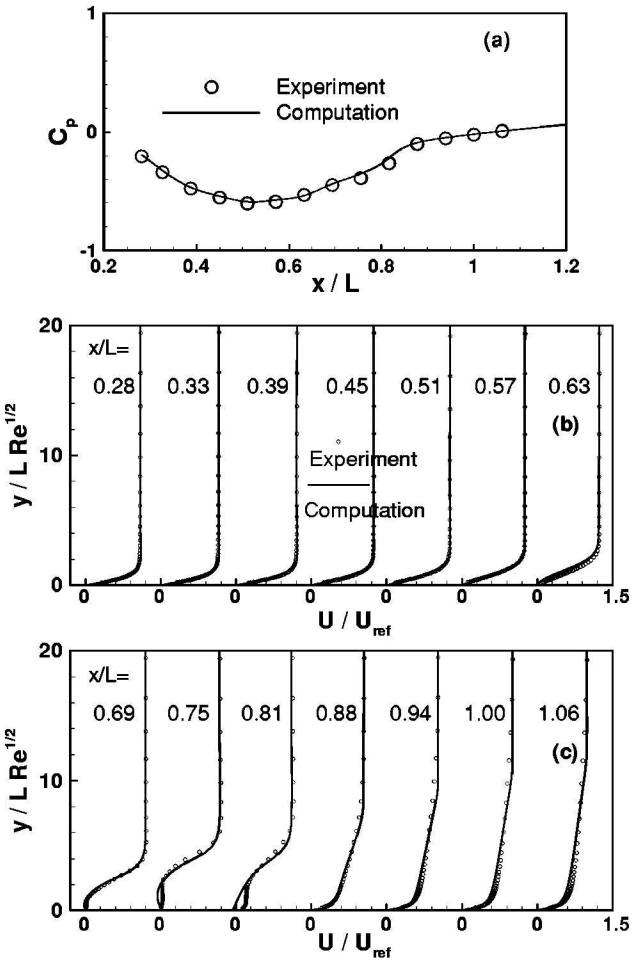

Fig. 12 Prediction of experiment of Hultgren and Volino [18]—Re=300,000, FSTI=0.2%

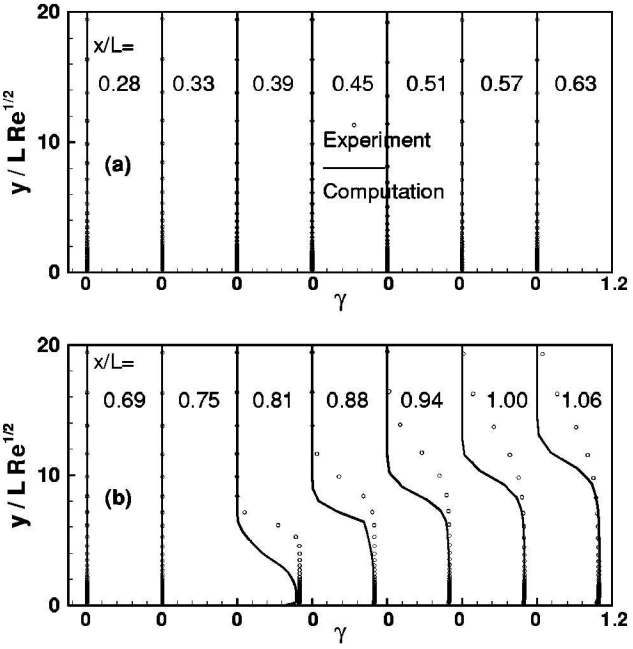

Fig. 13 Comparison of intermittency profiles along the surface—Re=300,000, FSTI=0.2%

bution is compared with experimental data, shown in Fig. 15(*a*). The agreement between the prediction and experimental data is very good.

The comparisons of the velocity profiles are shown in Figs. 15(*b*) and (*c*). As can be seen from the figures, good agreement is also observed for the velocity profiles. Once again, the discrepancy between the prediction and experiments near the wall is caused by the failure of the hot wire measurement in the separation region.

The intermittency profiles are compared to experimental data in Figs. 16(*a*) and (*b*). As can be seen from the figures, the flow remains laminar up to station $x/L=1.0$. At the last measurement station, $x/L=1.06$, the predicted intermittency factors show a larger magnitude than the experiments.

The turbulence intensity profiles are compared to experimental data in Figs. 17(*a*) and (*b*). It can be seen that the prediction gives rise to larger values of the turbulent kinetic energy profiles for region $x/L>0.65$. Even though the agreement is not that good, due to the fact that the transition only occurs at $x/L=1.03$ its impact to the velocity profiles is not that pronounced.

5 Concluding Remarks

A new transport equation for the intermittency factor is employed to predict a recent transitional boundary layer flow experiment under low pressure turbine airfoil conditions. The intermittent behavior of the transitional flows is taken into account by modifying the eddy viscosity with the intermittency factor. The new transport model not only can reproduce the experimentally observed streamwise variation of the intermittency in the transition zone, but also provides a realistic cross-stream variation of the intermittency profile. Computations are performed for two different Reynolds numbers and two different values of free stream turbulence intensities. Detailed comparisons with experiments are made for pressure coefficients, velocity, intermittency and turbulent kinetic energy profiles. Overall, good agreement with the experimental data is obtained. It has been demonstrated that the predictions accurately mimic the dynamic behavior of the inter-

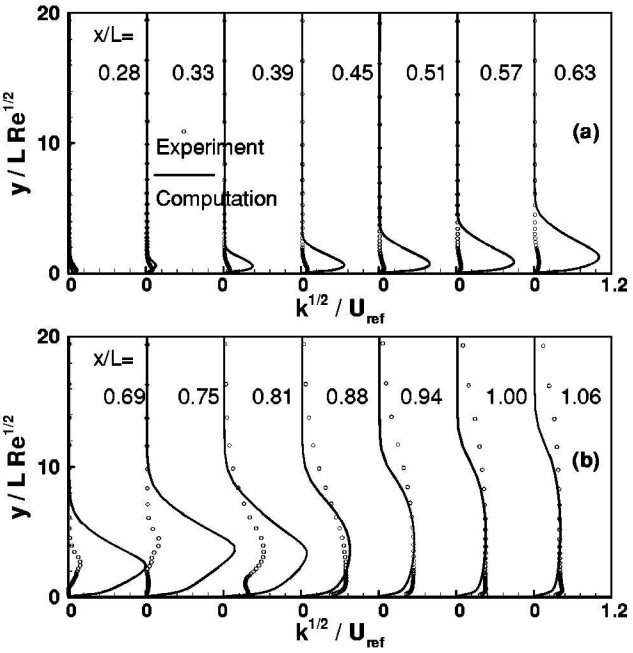

Fig. 14 Comparison of turbulence intensity profiles along the surface—Re=300,000, FSTI=0.2%

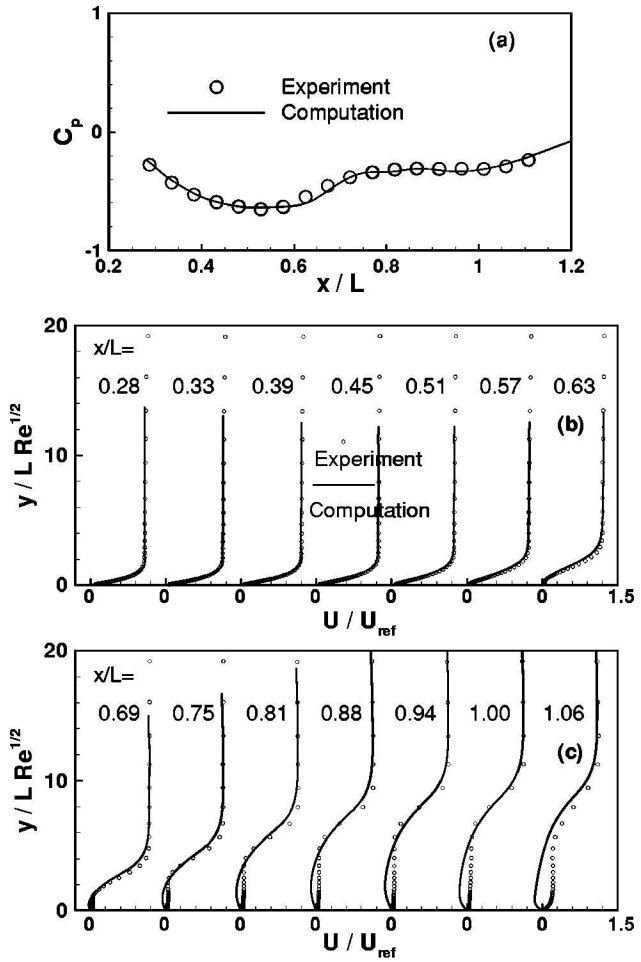

Fig. 15 Prediction of experiment of Hultgren and Volino [18]—Re=50,000, FSTI=0.2%

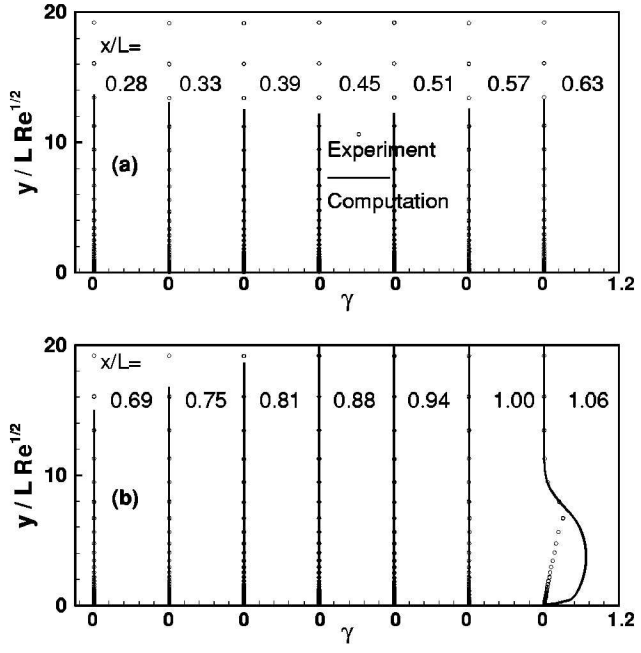

Fig. 16 Comparison of intermittency profiles along the surface—Re=50,000, FSTI=0.2%

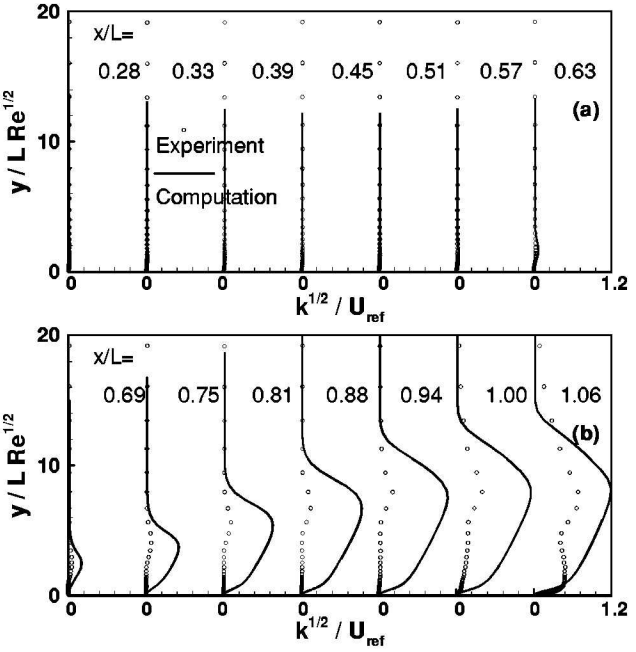

Fig. 17 Comparison of turbulence intensity profiles along the surface—Re=50,000, FSTI=0.2%

play between the transition and separation when subject to variations of Reynolds number and freestream turbulence intensity conditions.

Acknowledgments

This work is supported by NASA Glenn Research Center under grant NCC3-590. The project is part of the Low Pressure Turbine Flow Physics program of NASA-Glenn. This paper was originally published as AIAA Paper 2001-0446.

Nomenclature

C_p = pressure coefficient, $1-(U_e/U_{ref})^2$
FSTI = freestream turbulence intensity (%)
K_t = flow acceleration parameter, $(\nu/U^2)(dU/ds)$
k = turbulent kinetic energy
L = nominal suction surface wetted length
N = nondimensional spot breakdown rate parameter, $n\sigma\theta_t^3/\nu$
n = spot generation rate
p = static pressure
Re = Reynolds no., LU_{ref}/ν
Re_{st} = $(s_t-s_s)U_e/\nu$
$\mathrm{Re}_{\theta t}$ = $\theta_t U_e/\nu$
s = distance along streamwise coordinate
Tu = local turbulence intensity (%), u'/U
U = boundary layer streamwise velocity
U_e = local freestream velocity
U_{ref} = nominal exit freestream velocity
u_τ = friction velocity
W = magnitude of vorticity
x = wetted streamwise distance along suction surface
y_n = distance normal to wall
y^+ = $y_n u_\tau/\nu$
γ = intermittency factor
θ = momentum thickness
λ_θ = pressure gradient parameter, $(\theta^2/\nu)(dU/ds)$
μ = molecular viscosity
μ_t = eddy viscosity
ν = μ/ρ

ν_t = μ_t/ρ
ρ = density
σ = spot propagation parameter

Subscripts

e = freestream
s = onset of separation
t = onset of transition

References

[1] Mayle, R. E., 1991, "The Role of Laminar-Turbulent Transition in Gas Turbine Engines," ASME J. Turbomach., **113**, pp. 509–537.
[2] Rivir, R. B., 1996, "Transition on Turbine Blades and Cascades at Low Reynolds Numbers," AIAA Pap., AIAA-96-2079.
[3] Lake, J. P., King, P. I., and Rivir, R. B., 2000, "Low Reynolds Number Loss Reduction on Turbine Blades With Dimples and V-Grooves," AIAA Pap., AIAA-00-0738.
[4] Wisler, D. C., 1998, "The Technical and Economic Relevance of Understanding Boundary Layer Transition in Gas Turbine Engines," *Minnowbrook II-1997 Workshop on Boundary Layer Transition in Turbomachines*, eds., J. E. LaGraff and D. E. Ashpis, NASA CP-1998-206958, pp. 53–64.
[5] Savill, A. M., 1993, "Some Recent Progress in the Turbulence Modeling of By-pass Transition," *Near-Wall Turbulent Flows*, eds., R. M. C. So, C. G. Speziale, and B. E. Launder, Elsevier Science Publishers B. V., pp. 829–848.
[6] Savill, A. M., 1993, "Further Progress in The Turbulence Modeling of By-pass Transition," *Engineering Turbulence Modeling and Experiments 2*, eds., W. Rodi and F. Martelli, Elsevier Science Publishers B. V., pp. 583–592.
[7] Westin, K. J. A., and Henkes, R. A. W. M., 1997, "Application of Turbulence Models to Bypass Transition," ASME J. Fluids Eng., **119**, pp. 859–866.
[8] Dhawan, S., and Narasimha, R., 1958, "Some Properties of Boundary Layer During the Transition From Laminar to Turbulent Flow Motion," J. Fluid Mech., **3**, pp. 418–436.
[9] Gostelow, J. P., Blunden, A. R., and Walker, G. J., 1994, "Effects of Free-Stream Turbulence and Adverse Pressure Gradients on Boundary Layer Transition," ASME J. Turbomach., **116**, pp. 392–404.
[10] Solomon, W. J., Walker, G. J., and Gostelow, J. P., 1995, "Transition Length Prediction for Flows With Rapidly Changing Pressure Gradients," ASME Paper ASME-95-GT-241.
[11] Chen, K. K., and Thyson, N. A., 1971, "Extension of Emmons' Spot Theory to Flows on Blunt Bodies," AIAA J., **9**(5), pp. 821–825.
[12] Steelant, J., and Dick, E., 1996, "Modelling of Bypass Transition With Conditioned Navier-Stokes Equations Coupled to an Intermittency Transport Equation," Int. J. Numer. Methods Fluids, **23**, pp. 193–220.
[13] Cho, J. R., and Chung, M. K., 1992, "A $k-\epsilon-\gamma$ Equation Turbulence Model," J. Fluid Mech., **237**, pp. 301–322.
[14] Suzen, Y. B., and Huang, P. G., 1999, "Modelling of Flow Transition Using an Intermittency Transport Equation," NASA Contractor Report NASA-CR-1999-209313.
[15] Simon, T. W., Qiu, S., and Yuan, K., 2000, "Measurements in a Transitional Boundary Layer Under Low-Pressure Turbine Airfoil Conditions," NASA Contractor Report NASA-CR-2000-209957.
[16] Suzen, Y. B., and Huang, P. G., 2000, "Modelling of Flow Transition Using an Intermittency Transport Equation," ASME J. Fluids Eng., **122**, pp. 273–284.
[17] Suzen, Y. B., Xiong, G., and Huang, P. G., 2002, "Predictions of Transitional Flows in Low-Pressure Turbines Using an Intermittency Transport Equation," AIAA J., **40**(2), pp. 254–266.
[18] Hultgren, L. S., and Volino, R. J., 2000, "Separated and Transitional Boundary Layers Under Low-Pressure Turbine Airfoil Conditions," NASA TM, in preparation.
[19] Volino, R. J., and Hultgren, L. S., 2000, "Measurements in Separated and Transitional Boundary Layers Under Low-Pressure Turbine Airfoil Conditions," ASME/IGTI Paper 2000-GT-0260.
[20] Simon, F. F., and Stephens, C. A., 1991, "Modeling of the Heat Transfer in Bypass Transitional Boundary-Layer Flows," NASA Technical Paper 3170.
[21] Huang, P. G., and Coakley, T. J., 1992, "An Implicit Navier-Stokes Code for Turbulent Flow Modeling," AIAA Pap., AIAA-92-0547.
[22] Menter, F. R., 1994, "Two-Equation Eddy-Viscosity Turbulence Models for Engineering Applications," AIAA J., **32**(8), pp. 1598–1605.
[23] Abu-Ghannam, B. J., and Shaw, R., 1980, "Natural Transition of Boundary Layers-The Effects of Turbulence, Pressure Gradient, and Flow History," J. Mech. Eng. Sci., **22**(5), pp. 213–228.
[24] Roberts, W. B., 1980, "Calculation of Laminar Separation Bubbles and Their Effect on Airfoil Performance," AIAA J., **18**(1), pp. 25–31.
[25] Davis, R. L., Carter, J. E., and Reshotko, E., 1987, "Analysis of Transitional Separation Bubbles on Infinite Swept Wings," AIAA J., **25**(3), pp. 421–428.
[26] Lake, J. P., 1999, "Flow Separation Prevention on a Turbine Blade at Low Reynolds Number," Ph.D. dissertation, Air Force Institute of Technology, Dayton, OH.